Journal of Solid Mechanics Vol. 12, No. 1 (2020) pp. 1-15
DOI: 10.22034/jsm.2020.670341

Temperature-Dependent Buckling Analysis of Functionally Graded Sandwich Cylinders

Y. Mohammadi [*] , M. Rahmani

Faculty of Industrial and Mechanical Engineering, Qazvin Branch, Islamic Azad University, Qazvin, Iran

Received 1 September 2019; accepted 17 November 2019

ABSTRACT

This study is limited to study of buckling analysis of a sandwich cylindrical shell with functionally graded face sheets and homogenous core. High-order sandwich plate theory is improved by considering the in-plane stresses of the core that usually are ignored in the analysis of sandwich structures. Assume that all properties of the face sheets and the core are temperature dependent. Strain components are obtained by using the nonlinear Von-Karman type relations. The equilibrium equations are derived via principle of minimum potential energy. Analytical solution for static analysis of simply supported sandwich conical shells with functionally graded face sheets under axial in-plane compressive loads and in the temperature environments is performed by using Navier's solution. The results show the critical dimensionless static axial loads are affected by the configurations of the constituent materials, compositional profile variations, temperature and the variation of the sandwich geometry. The comparisons show that the present results are in the good agreement with the numerical results.

Keywords: Buckling; Sandwich cylinder; Temperature-dependent properties; Functionally graded.

1 INTRODUCTION

DUE to the advantages of being able to withstand a severe high-temperature gradient while maintaining structural integrity, functionally graded materials (FGMs) have been receiving much more attention in engineering communities, especially in applications for high-temperature environment such as nuclear reactors, space planes and chemical plants. Functionally graded materials are microscopically inhomogeneous composite materials, in which the mechanical properties vary smoothly and continuously from one surface to the other [1]. Composition is varied with continuous changes in the volume fraction of constituent materials. These materials are usually made from a mixture of metals and ceramics through a powder metallurgy process. The advantage of using these materials is that they are able to withstand high temperature gradient environment while maintaining their structural integrity. For example, the insulating tile for a re-entry space vehicle can be designed such that the outside is a refractory (ceramic) material, and the inside a load-carrying structure made of a strong and tough metal [1]. In recent years, functionally graded materials (FGMs) have been developed due to their excellent mechanical and

[*]Corresponding author.
E-mail address: u.mohammadi@gmail.com (Y. Mohammadi).

thermal properties. Sandwich structures find an increasing use in aerospace, naval, transportation, and other industries, which require stiff and lightweight structural components. Various theoretical models have been developed in the recent years to discuss the static and dynamic behavior of sandwich structures. These theories assume that the height of the core remains unchanged. A summary of classical theories can be found in the textbooks written by Plantema [2], Allen [3], and Zenkert [4]. Javaheri and Eslami studied the stability of FG rectangular plates under thermal loads by using the classical plate theory [5]. Zhao et al. investigated the mechanical and thermal buckling of FG plates by using the FSDT and element free kp-Ritz method. Exponential distribution is applied to model the variation of material properties [6]. Amir et al. studied the buckling behavior of nano composite sandwich plates by using first order shear deformation theory. The faces are piezoelectric and the flexoelectric effect was considered [7]. Bouderba et al. investigated the thermal buckling of FG sandwich plates with various boundary conditions by applying FSDT. The core was homogeneous and a power law distribution was used to show the variation of the materials [8]. Amir studied the vibration and instability of orthotropic grapheme sheet subjected to thermo magnetic field by using FSDT. Also, orthotropic visco Pasternak foundation was considered [9]. Sepiani et al. analyzed the free vibration and buckling of FG cylindrical shell under combined forces. FG materials were considered temperature dependent and varied with a power law distribution in the thickness direction. The equations are obtained based on FSDT by considering the transverse shear strains and rotary inertia [10]. Amir et al. studied the vibration of a porous rectangular plate with two piezo-electromagnetic face sheets resting on Winkler Pasternak foundation by applying the two variables sinusoidal shear deformation plate theory and a nonlocal theory [11]. Classical theories can often accurately determine the global response of the sandwich structure, for example, fundamental vibration frequencies. Modern sandwich structures are usually made of two metallic or laminated composite face sheets and a foam or low strength honeycomb core. These types of cores are flexible in all directions while upper and lower faces of the sandwich structure exhibit different deformation patterns. These effects denoted as localized effects cannot be accurately determined using classical sandwich theories. In order to take into account the compressibility of the core, a high-order sandwich theory has been developed by Frostig et al. [12]. High-order theory has successfully been used to analyze various problems of sandwich structures [13-18]. Seidi et al. by using a high order theory studied the buckling of truncated conical sandwich shells. The material of FG face sheets and homogenous core were temperature dependent [19]. Cylindrical shells are widely used in many engineering fields such as aerospace, chemical, civil, mechanical, naval, and nuclear. A predominant failure mode of axially compressed thin cylindrical shells is axial buckling, and this problem has been studied for more than a century [20–33]. For example, Winterstetter and Schmidt [23] have conducted a comprehensive experimental and numerical investigation of the buckling of a steel cylindrical shell under combined loading. Kim and Kim [24] used the commercial finite element code ABAQUS to analyze the effect of geometric imperfections on the buckling of axially compressed cylindrical shells and tanks. Pinna and Ronalds [25] have studied numerically the buckling and post-buckling of cylindrical shells with one end pinned and the other free, and computed the collapse and bifurcation loads. Eslami [27, 28] employed the Wan-Donnell and Koiter shell theories to investigate buckling deformations of isotropic and orthotropic laminated cylindrical shells subjected to mechanical and thermal loads. Mushtari and Sachenkov [29] investigated the buckling behavior of cylindrical and conical shells under external pressure. Lopatin and Morozov [30] presented an approximate analytical solution for the buckling problem of a composite sandwich cylindrical shell subjected to a uniform external lateral pressure. Malinowski et al. [31] analyzed the buckling and post-buckling problems of an elastic seven-layered cylindrical shell under uniformly distributed pressure. The buckling problems of functionally graded cylindrical shells are solved by a number of authors. For example, Shen [32, 33] used the perturbation method to analyze the thermal post-buckling of axially loaded and pressure-loaded cylindrical shells made of functionally graded materials. Li and Batra [34] studied the buckling of a simply-supported three-layer cylindrical shell under the axial compressive load. The inner and outer layers of the shell are comprised of the same homogeneous and isotropic material, and the middle layer is made of a functionally graded material. Sofiyev [35] discussed the vibration and buckling of sandwich cylindrical shells covered by different types of coatings, such as functionally graded, metal and ceramic coatings, and subjected to a uniform hydrostatic pressure. Shahsiah and Eslami [36] investigated thermal buckling behavior of functionally graded cylindrical shell based on improved Donnell equations. Woo et al. [37] provided an analytical solution for the post buckling behavior of moderately thick plates and shallow shells made of functionally graded materials under edge compressive loads and a temperature field. Ravikiran and Ganesan [38] studied linear thermal buckling and free vibration of functionally graded cylindrical shells with clamped–clamped boundary conditions based on temperature-dependent material properties.

But, there are no studies in the open literature on the buckling analysis of sandwich cylindrical shells with FG face sheets and temperature-dependent properties. In this study, a new improved high-order theory is presented for axial and thermal overall buckling analysis of sandwich cylindrical shells with FG face sheets and homogenous core.

First-order shear deformation plate theory is used for the face sheets and cubic functions are assumed for the transverse and in-plane displacements of the core. Strain components are calculated by use of nonlinear von Kármán relations. Continuity conditions of transverse shear stresses at the interface as well as the condition of zero transverse shear stresses on the upper and lower surface of the cylinder are satisfied. Also, transverse flexibility of the core and consequently the core transverse normal strain and stress are considered. The equation of motion and boundary conditions are derived via principle of minimum potential energy. Analytical solution for static analysis of sandwich cylinders with simply-supported boundary conditions under axial in-plane compressive loads is presented using Navier's solution.

2 STRUCTURE AND MATERIAL

A sandwich cylinder with functionally graded face sheets is considered under axial loads, see Fig. 1. h_0 and h_i are the thicknesses of the outer and inner FG face sheets, respectively, and *R* indicate the radius of the cylinder. The face sheets material are assumed to be functionally graded and the core is assumed as homogeneous material with thickness of h_c . The properties of the FG face sheets, $p\left(z_j,T\right)$, such as Young's modulus, Poisson's ratio, thermal expansion coefficient and the density of FG face sheets, are introduced by power-law function as:

$$\begin{aligned} &P(z_j,T)=g(z_j)P_{ce}^{j}(T)+[1-g(z_j)]P_m^j(T) \quad , \quad j=(o,i) \\ &g(z_o)=\left(\frac{h_o/2-z_o}{h_o}\right)^N \ , \ g(z_i)=\left(\frac{h_i/2+z_i}{h_i}\right)^N \end{aligned} \tag{1}$$

where $P_{ce}^{j}(T)$ and $P_m^j(T)$ are the materials properties of the ceramic and metal, respectively. And they are expressed as a function of temperature as [39]

$$P_{ce}^{j} \text{ or } P_m^j = C_0\left(C_{-1}T^{-1}+1+C_1T+C_2T^2+C_3T^3\right) \tag{2}$$

where *T* is temperature and is expressed in Kelvin; C_0,C_{-1},C_1,C_2,C_3 are the coefficients and are unique to the constituent materials [40].

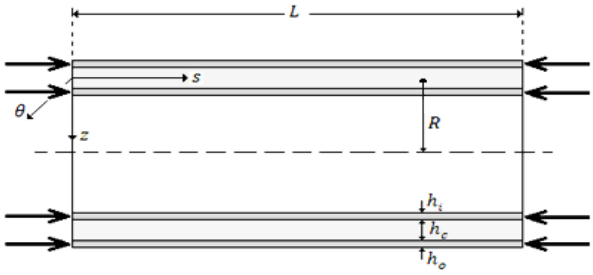

Fig.1
Two-dimensional view of sandwich cylinder with axial in-plane compressive load.

3 FORMULATION

In the present paper, the first shear deformation theory is adopted for the face sheets:

$$\begin{aligned} &u_j(s,\theta,z_j)=u_{0j}(s,\theta)+z_j\varphi_s^j(s,\theta) \\ &v_j(s,\theta,z_j)=v_{0j}(s,\theta)+z_j\varphi_\theta^j(s,\theta) \quad ,j=(o,i) \\ &w_j(s,\theta,z_j)=w_{0j}(s,\theta) \end{aligned} \tag{3}$$

where u_0, v_0 and w_0 are displacements of mid-surface along the s, θ and z direction and φ_s^j and φ_θ^j are rotations of the normal to the mid-surface along θ and s axis, respectively. The core layer is much thicker and softer than the face sheets. Thus, the displacement fields for the core are assumed as a cubic pattern for the in-plane and vertical displacement components [41]:

$$\begin{aligned} u_c(s,\theta,z_c) &= u_0(s,\theta)+u_1(s,\theta)z_c+u_2(s,\theta){z_c}^2+u_3(s,\theta){z_c}^3 \\ v_c(s,\theta,z_c) &= v_0(s,\theta)+v_1(s,\theta)z_c+v_2(s,\theta){z_c}^2+v_3(s,\theta){z_c}^3 \\ w_c(s,\theta,z_c) &= w_0(s,\theta)+w_1(s,\theta)z_c+w_2(s,\theta){z_c}^2+w_3(s,\theta){z_c}^3 \end{aligned} \tag{4}$$

where u_k and v_k (k=0, 1, 2, 3) are the unknowns of the in-plane displacement components of the core and w_k (k=0, 1, 2, 3) are the unknowns of its vertical displacements, respectively. In this model, there are twenty eight unknowns: ten displacement unknowns for both face sheets, twelve displacement unknowns for the core, and six Lagrange multipliers.

In the present model, assumed core is perfectly bonded to the face sheets. Hence, there are three interface displacements in each face sheet-core interface, which can be obtained as follows:

$$\begin{aligned} &u_o(z_o=h_o/2)=u_c(z_c=-h_c/2),\ \ v_o(z_o=h_o/2)=v_c(z_c=-h_c/2),\ \ w_o=w_c(z_c=-h_c/2), \\ &u_c(z_c=h_c/2)=u_i(z_i=-h_i/2), v_c(z_c=h_c/2)=v_i(z_i=-h_i/2), w_c(z_c=h_c/2)=w_i \end{aligned} \tag{5}$$

The nonlinear von Kármán strain-displacement relations for the face sheets (j=o , i) can be defined as:

$$\begin{aligned} \varepsilon_{ss}^j &= u_{0j,s}+z_j\varphi_{s,s}^j+\frac{1}{2}w_{j,s}^2-\alpha_j\Delta T_j \\ \varepsilon_{\theta\theta}^j &= \frac{1}{r}\left(v_{0j,\theta}+z_j\varphi_{\theta,\theta}^j+w_j\right)+\frac{1}{2r^2}w_{j,\theta}^2-\alpha_j\Delta T_j \\ \varepsilon_{zz}^j &= -\alpha_j\Delta T_j \qquad\qquad j=(o,i) \\ \gamma_{s\theta}^j &= \frac{1}{r}\left(u_{0j,\theta}+z_j\varphi_{s,\theta}^j\right)+v_{0j,s}+z_j\varphi_{\theta,s}^j+\frac{1}{r}w_{j,s}w_{j,\theta} \\ \gamma_{sz}^j &= \varphi_s^j+w_{j,s} \\ \gamma_{\theta z}^j &= \frac{1}{r}\left(w_{j,\theta}-v_{0j}-z_j\varphi_\theta^j\right)+\varphi_\theta^j \end{aligned} \tag{6}$$

In addition, the nonlinear von Kármán strain-displacement relations for the core can be expressed as:

$$\begin{aligned} \varepsilon_{ss}^c &= u_{0,s}+u_{1,s}z_c+u_{2,s}{z_c}^2+u_{3,s}{z_c}^3+\frac{1}{2}{w_{0,s}}^2-\alpha_c\Delta T_c \\ \varepsilon_{\theta\theta}^c &= \frac{1}{r}\left[v_{0,\theta}+v_{1,\theta}z_c+v_{2,\theta}{z_c}^2+v_{3,\theta}{z_c}^3+\left(w_0+w_1z_c+w_2{z_c}^2+w_3{z_c}^3\right)\right]+\frac{1}{2r^2}{w_{0,\theta}}^2-\alpha_c\Delta T_c \\ \varepsilon_{zz}^c &= w_1+2w_2z_c+3w_3{z_c}^2-\alpha_c\Delta T_c \\ \gamma_{sz}^c &= \left(u_1+2u_2z_c+3u_3{z_c}^2\right)+\left(w_{0,s}+w_{1,s}z_c+w_{2,s}{z_c}^2+w_{3,s}{z_c}^3\right) \\ \gamma_{\theta z}^c &= \frac{1}{r}\left[w_{0,\theta}+w_{1,\theta}z_c+w_{2,\theta}{z_c}^2+w_{3,\theta}{z_c}^3-\left(v_0+v_1z_c+v_2{z_c}^2+v_3{z_c}^3\right)\right]+v_1+2v_2z_c+3v_3{z_c}^2 \\ \gamma_{s\theta}^c &= \frac{1}{r}\left[u_{0,\theta}+u_{1,\theta}z_c+u_{2,\theta}{z_c}^2+u_{3,\theta}{z_c}^3+w_{0,s}w_{0,\theta}\right]+v_{0,s}+v_{1,s}z_c+v_{2,s}{z_c}^2+v_{3,s}{z_c}^3 \end{aligned} \tag{7}$$

For determination of stress resultants for each FG face sheet (j=o , i) constitutive equations are as follows:

$$\begin{Bmatrix} N_{ss}^{j} \\ N_{\theta\theta}^{j} \\ N_{s\theta}^{j} \end{Bmatrix} = \begin{bmatrix} A_{11} & A_{12} & 0 \\ A_{12} & A_{22} & 0 \\ 0 & 0 & A_{66} \end{bmatrix} \begin{Bmatrix} \varepsilon_{ssj}^{(0)} \\ \varepsilon_{\theta\theta j}^{(0)} \\ \varepsilon_{s\theta j}^{(0)} \end{Bmatrix} + \begin{bmatrix} B_{11} & B_{12} & 0 \\ B_{12} & B_{22} & 0 \\ 0 & 0 & B_{66} \end{bmatrix} \begin{Bmatrix} \varepsilon_{ssj}^{(1)} \\ \varepsilon_{\theta\theta j}^{(1)} \\ \varepsilon_{s\theta j}^{(1)} \end{Bmatrix} - \begin{Bmatrix} N_{ss}^{Tj} \\ N_{\theta\theta}^{Tj} \\ 0 \end{Bmatrix}$$

$$\begin{Bmatrix} M_{ss}^{j} \\ M_{\theta\theta}^{j} \\ M_{s\theta}^{j} \end{Bmatrix} = \begin{bmatrix} B_{11} & B_{12} & 0 \\ B_{12} & B_{22} & 0 \\ 0 & 0 & B_{66} \end{bmatrix} \begin{Bmatrix} \varepsilon_{ssj}^{(0)} \\ \varepsilon_{\theta\theta j}^{(0)} \\ \varepsilon_{s\theta j}^{(0)} \end{Bmatrix} + \begin{bmatrix} D_{11} & D_{12} & 0 \\ D_{12} & D_{22} & 0 \\ 0 & 0 & D_{66} \end{bmatrix} \begin{Bmatrix} \varepsilon_{ssj}^{(1)} \\ \varepsilon_{\theta\theta j}^{(1)} \\ \varepsilon_{s\theta j}^{(1)} \end{Bmatrix} - \begin{Bmatrix} M_{ss}^{Tj} \\ M_{\theta\theta}^{Tj} \\ 0 \end{Bmatrix} \tag{8}$$

$$\begin{Bmatrix} Q_{sj}^{(0)} \\ Q_{\theta j}^{(0)} \end{Bmatrix} = \frac{\pi^2}{12} \begin{bmatrix} A_{44} & 0 \\ 0 & A_{55} \end{bmatrix} \begin{Bmatrix} \gamma_{szj}^{(0)} \\ \gamma_{\theta zj}^{(0)} \end{Bmatrix} + \frac{\pi^2}{12} \begin{bmatrix} B_{44} & 0 \\ 0 & B_{55} \end{bmatrix} \begin{Bmatrix} \gamma_{szj}^{(1)} \\ \gamma_{\theta zj}^{(1)} \end{Bmatrix} \quad , \qquad j = (o, i)$$

$$Q_{\theta j}^{(1)} = \frac{\pi^2}{12} B_{55} \gamma_{\theta zj}^{(0)} + \frac{\pi^2}{12} D_{55} \gamma_{\theta zj}^{(1)} \quad , \qquad j = (o, i)$$

It should be noted that $\frac{\pi^2}{12}$ is the shear correction factor of FSDT. In addition, the strain components for a sandwich cylinder are defined as:

$$\begin{Bmatrix} \varepsilon_{ssj}^{(0)} \\ \varepsilon_{\theta\theta j}^{(0)} \\ \varepsilon_{s\theta j}^{(0)} \end{Bmatrix} = \begin{Bmatrix} u_{0j,s} + \frac{1}{2} w_{j,s}{}^2 \\ \frac{1}{r}\left(v_{0j,\theta} + w_j\right) + \frac{1}{2r^2} w_{j,\theta}{}^2 \\ \frac{1}{r} u_{0j,\theta} + v_{0j,s} + \frac{1}{r} w_{j,s} w_{j,\theta} \end{Bmatrix} \quad , \quad \begin{Bmatrix} \varepsilon_{ssj}^{(1)} \\ \varepsilon_{\theta\theta j}^{(1)} \\ \varepsilon_{s\theta j}^{(1)} \end{Bmatrix} = \begin{Bmatrix} \varphi_{s,s}^{j} \\ \frac{1}{r} \varphi_{\theta,\theta}^{j} \\ \frac{1}{r} \varphi_{s,\theta}^{j} + \varphi_{\theta,s}^{j} \end{Bmatrix}$$

$$\begin{Bmatrix} \gamma_{szj}^{(0)} \\ \gamma_{\theta zj}^{(0)} \end{Bmatrix} = \begin{Bmatrix} w_{j,s} + \varphi_s^j \\ \frac{1}{r}\left(w_{j,\theta} - v_{0j}\right) + \varphi_\theta^j \end{Bmatrix} \quad , \quad \begin{Bmatrix} \gamma_{szj}^{(1)} \\ \gamma_{\theta zj}^{(1)} \end{Bmatrix} = \begin{Bmatrix} 0 \\ \frac{-\varphi_\theta^j}{r} \end{Bmatrix} \tag{9}$$

Also, $N_{ss}^{Tj}, N_{\theta\theta}^{Tj}, M_{ss}^{Tj}$ and $M_{\theta\theta}^{Tj}$ are the thermal stress resultants and A_{kl}^{j}, B_{kl}^{j} and $D_{kl}^{j}, (k, l = 1,2,6)$ are the stiffness matrices components that for the outer and the inner face sheets are as follows:

$$N_{ss}^{Tj} = N_{\theta\theta}^{Tj} = \int_{-\frac{h_j}{2}}^{\frac{h_j}{2}} \frac{E_j(z_j, T_j)}{1 - \upsilon_j(z_j, T_j)} . \alpha_j(z_j, T_j) . \Delta T_j \, dz_j \quad , \quad j = (o, i)$$

$$M_{ss}^{Tj} = M_{\theta\theta}^{Tj} = \int_{-\frac{h_j}{2}}^{\frac{h_j}{2}} \frac{z_j . E_j(z_j, T_j)}{1 - \upsilon_j(z_j, T_j)} . \alpha_j(z_j, T_j) . \Delta T_j \, dz_j \quad , \quad j = (o, i)$$

$$\begin{Bmatrix} A_{11}^{j} \\ B_{11}^{j} \\ D_{11}^{j} \end{Bmatrix} = \begin{Bmatrix} A_{22}^{j} \\ B_{22}^{j} \\ D_{22}^{j} \end{Bmatrix} = \int_{-\frac{h_j}{2}}^{\frac{h_j}{2}} \left[\frac{E_j\left(z_j, T_j\right)}{1 - \left(\vartheta_j\left(z_j, T_j\right)\right)^2} \right] \begin{Bmatrix} 1 \\ z_j \\ z_j^{\,2} \end{Bmatrix} dz_j$$

$$\begin{Bmatrix} A_{12}^{j} \\ B_{12}^{j} \\ D_{12}^{j} \end{Bmatrix} = \int_{-\frac{h_j}{2}}^{\frac{h_j}{2}} \left[\frac{\vartheta_j\left(z_j, T_j\right) \times E_j\left(z_j, T_j\right)}{1 - \left(\vartheta_j\left(z_j, T_j\right)\right)^2} \right] \begin{Bmatrix} 1 \\ z_j \\ z_j^{\,2} \end{Bmatrix} dz_j \tag{10}$$

$$\begin{Bmatrix} A_{66}^{j} \\ B_{66}^{j} \\ D_{66}^{j} \end{Bmatrix} = \int_{-\frac{h_j}{2}}^{\frac{h_j}{2}} \left[\frac{E_j\left(z_j, T_j\right)}{2\left(1 + \vartheta_j\left(z_j, T_j\right)\right)} \right] \begin{Bmatrix} 1 \\ z_j \\ z_j^{\,2} \end{Bmatrix} dz_j$$

where $E_j\left(z_j,T_j\right),\vartheta_j\left(z_j,T_j\right)$ and $\alpha_j\left(z_j,T_j\right)$, $j=(o,i)$ are the modulus of elasticity, Poisson's ratio and the thermal expansion coefficient of the FG face sheets, respectively, and introduced by power-law function of FGMs. "*o*" and "*i*" refer to the outer and inner face sheet layers, respectively. In addition, twenty-three stress resultants of the core are defined as:

$$\left\{Q_{sz}^{c},M_{Q1sz}^{c},M_{Q2sz}^{c},M_{Q3sz}^{c}\right\}=\int_{-\frac{h_c}{2}}^{\frac{h_c}{2}}\left(1,z_c,{z_c}^2,{z_c}^3\right)\tau_{sz}^{c}dz_c$$

$$\left\{Q_{\theta z}^{c},M_{Q1\theta z}^{c},M_{Q2\theta z}^{c},M_{Q3\theta z}^{c}\right\}=\int_{-\frac{h_c}{2}}^{\frac{h_c}{2}}\left(1,z_c,{z_c}^2,{z_c}^3\right)\tau_{\theta z}^{c}dz_c$$

$$\left\{R_{z}^{c},M_{z1}^{c},M_{z2}^{c}\right\}=\int_{-\frac{h_c}{2}}^{\frac{h_c}{2}}\left(1,z_c,{z_c}^2\right)\sigma_{zz}^{c}dz_c$$

$$\left\{Q_{s\theta}^{c},M_{Q1s\theta}^{c},M_{Q2s\theta}^{c},M_{Q3s\theta}^{c}\right\}=\int_{-\frac{h_c}{2}}^{\frac{h_c}{2}}\left(1,z_c,{z_c}^2,{z_c}^3\right)\tau_{s\theta}^{c}dz_c \tag{11}$$

$$\left\{R_{s}^{c},M_{s1}^{c},M_{s2}^{c},M_{s3}^{c}\right\}=\int_{-\frac{h_c}{2}}^{\frac{h_c}{2}}\left(1,z_c,{z_c}^2,{z_c}^3\right)\sigma_{ss}^{c}dz_c$$

$$\left\{R_{\theta}^{c},M_{\theta1}^{c},M_{\theta2}^{c},M_{\theta3}^{c}\right\}=\int_{-\frac{h_c}{2}}^{\frac{h_c}{2}}\left(1,z_c,{z_c}^2,{z_c}^3\right)\sigma_{\theta\theta}^{c}dz_c$$

4 GOVERNING EQUATIONS

The governing equations are derived through the principle of minimum potential energy:

$$\delta U+\delta V=0 \tag{12}$$

where U is the total strain energy, V is the total potential energy and δ denotes the variation operator. The total potential energy is equals to:

$$\delta V=-\int_0^L\int_0^{2\pi}(n_s^o\delta u_{0o}+n_s^i\delta u_{0i})r\,d\theta ds \tag{13}$$

where u_{oo},u_{oi} are mid-plane displacements of the outer and inner face sheets in the longitudinal direction, respectively. n_s^o and n_s^i are the in-plane external loads of the outer and inner face sheets, respectively. In addition, the first variation of the total strain energy is as follows:

$$
\begin{aligned}
\delta U = & \int_{V_o} \left(\sigma_{ss}^{o}\, \delta\varepsilon_{ss}^{o} + \sigma_{\theta\theta}^{o}\, \delta\varepsilon_{\theta\theta}^{o} + \tau_{s\theta}^{o}\, \delta\gamma_{s\theta}^{o} + \tau_{sz}^{o}\, \delta\gamma_{sz}^{o} + \tau_{\theta z}^{o}\, \delta\gamma_{\theta z}^{o} \right) dV \\
& + \int_{V_i} \left(\sigma_{ss}^{i}\, \delta\varepsilon_{ss}^{i} + \sigma_{\theta\theta}^{i}\, \delta\varepsilon_{\theta\theta}^{i} + \tau_{s\theta}^{i}\, \delta\gamma_{s\theta}^{i} + \tau_{sz}^{i}\, \delta\gamma_{sz}^{i} + \tau_{\theta z}^{i}\, \delta\gamma_{\theta z}^{i} \right) dV \\
& + \int_{V_{core}} \left(\tau_{sz}^{c}\, \delta\gamma_{sz}^{c} + \tau_{\theta z}^{c}\, \delta\gamma_{\theta z}^{c} + \sigma_{zz}^{c}\, \delta\varepsilon_{zz}^{c} + \sigma_{ss}^{c}\, \delta\varepsilon_{ss}^{c} + \sigma_{\theta\theta}^{c}\, \delta\varepsilon_{\theta\theta}^{c} + \tau_{s\theta}^{c}\, \delta\gamma_{s\theta}^{c} \right) dV \\
& + \delta \int_0^L \int_0^{2\pi} \Big[\lambda_{so} \left(u_o \left(z_o = h_O/2 \right) - u_c \left(z_c = -h_c/2 \right) \right) + \lambda_{\theta o} \left(v_o \left(z_o = h_o/2 \right) - v_c \left(z_c = -h_c/2 \right) \right) \\
& + \lambda_{zo} \left(w_o - w_c \left(z_c = -h_c/2 \right) \right) + \lambda_{si} \left(u_c \left(z_c = h_c/2 \right) - u_i \left(z_i = -h_i/2 \right) \right) \\
& + \lambda_{\theta i} \left(v_c \left(z_c = h_c/2 \right) - v_i \left(z_i = -h_i/2 \right) \right) + \lambda_{zi} \left(w_c \left(z_c = h_c/2 \right) - w_i \right) \Big] r\, d\theta\, ds
\end{aligned}
\tag{14}
$$

where σ_{ss}^{j} and $\sigma_{\theta\theta}^{j}$ (j=o, i) are the in-plane normal stresses and ε_{ss}^{j} and $\varepsilon_{\theta\theta}^{j}$ (j=o, i) are the in-plane normal strains of the outer and inner face sheets; $\sigma_{ss}^{c}, \sigma_{\theta\theta}^{c}, \varepsilon_{\theta\theta}^{c}$ and ε_{ss}^{c} are the in-plane normal stresses and strains of the core, respectively; $\tau_{s\theta}^{j}$ and $\gamma_{s\theta}^{j}$ (j=o, i, c) are the in-plane shear stresses and strains in the face sheets and the core; σ_{zz}^{c} and ε_{zz}^{c} are the normal stress and normal strain in the vertical direction of the core; τ_{sz}^{c} and γ_{sz}^{c} are the vertical shear stress and vertical shear strain in the core; V_0, V_i and V_{core} are the volume of outer and inner face sheets and the core, respectively; $\lambda_{sj}, \lambda_{\theta j}$ and λ_{zj} (j=o, i) are six Lagrange multipliers for compatibility conditions at the outer and inner face sheet-core interfaces. By using the Eqs. (12, 13, 14) and after some algebraic manipulation, the twenty eight equations of equilibrium are calculated as follows:

Five equations for the outer FG face sheet:

$$
\begin{aligned}
& r N_{ss,s}^{o} + N_{s\theta,\theta}^{o} - r\lambda_{so} + r m_s^{o} = 0 \\
& N_{\theta\theta,\theta}^{o} + r N_{s\theta,s}^{o} + Q_{\theta o}^{(0)} \cos\beta - r\lambda_{\theta o} = 0 \\
& -N_{\theta\theta}^{o} + r Q_{so,s}^{(0)} + Q_{\theta o,\theta}^{(0)} + N\left(w_o\right) - r\lambda_{zo} = 0 \\
& r M_{ss,s}^{o} + M_{s\theta,\theta}^{o} - r Q_{so}^{(0)} - r\lambda_{so} \frac{h_o}{2} = 0 \\
& M_{\theta\theta,\theta}^{o} + r M_{s\theta,s}^{o} - r Q_{\theta o}^{(0)} + Q_{\theta o}^{(1)} - r\lambda_{\theta o} \frac{h_o}{2} = 0
\end{aligned}
\tag{15}
$$

Five equations for the inner FG face sheet:

$$
\begin{aligned}
& r N_{ss,s}^{i} + N_{s\theta,\theta}^{i} + r\lambda_{si} + r m_s^{i} = 0 \\
& N_{\theta\theta,\theta}^{i} + r N_{s\theta,s}^{i} + Q_{\theta i}^{(0)} + r\lambda_{\theta i} = 0 \\
& -N_{\theta\theta}^{i} + r Q_{si,s}^{(0)} + Q_{\theta i,\theta}^{(0)} + N\left(w_i\right) + r\lambda_{zi} = 0 \\
& r M_{ss,s}^{i} + M_{s\theta,\theta}^{i} - r Q_{si}^{(0)} - r\lambda_{si} \frac{h_i}{2} = 0 \\
& M_{\theta\theta,\theta}^{i} + r M_{s\theta,s}^{i} - r Q_{\theta i}^{(0)} + Q_{\theta i}^{(1)} - r\lambda_{\theta i} \frac{h_i}{2} = 0
\end{aligned}
\tag{16}
$$

Twelve equations for the core:

$$
\begin{aligned}
&rR^{c}_{s,s}+Q^{c}_{s\theta,\theta}+r\lambda_{so}-r\lambda_{si}=0\\
&-rQ^{c}_{sz}+rM^{c}_{s1,s}+M^{c}_{Q1s\theta,\theta}-r\lambda_{so}\frac{h_c}{2}-r\lambda_{si}\frac{h_c}{2}=0\\
&-2rM^{c}_{Q1sz}+rM^{c}_{s2,s}+M^{c}_{Q2s\theta,\theta}+r\lambda_{so}\frac{h_c^{2}}{4}-r\lambda_{si}\frac{h_c^{2}}{4}=0\\
&-3rM^{c}_{Q2sz}+rM^{c}_{s3,s}+M^{c}_{Q3s\theta,\theta}-r\lambda_{so}\frac{h_c^{3}}{8}-r\lambda_{si}\frac{h_c^{3}}{8}=0\\
&Q^{c}_{\theta z}+R^{c}_{\theta,\theta}+rQ^{c}_{s\theta,s}+r\lambda_{\theta o}-r\lambda_{\theta i}=0\\
&M^{c}_{Q1\theta z}-rQ^{c}_{\theta z}+M^{c}_{\theta1,\theta}+rM^{c}_{Q1s\theta,s}-r\lambda_{\theta o}\frac{h_c}{2}-r\lambda_{\theta i}\frac{h_c}{2}=0\\
&M^{c}_{Q2\theta z}-2rM^{c}_{Q1\theta z}+M^{c}_{\theta2,\theta}+rM^{c}_{Q2s\theta,s}+r\lambda_{\theta o}\frac{h_c^{2}}{4}-r\lambda_{\theta i}\frac{h_c^{2}}{4}=0\\
&M^{c}_{Q3\theta z}-3rM^{c}_{Q2\theta z}+M^{c}_{\theta3,\theta}+rM^{c}_{Q3s\theta,s}-r\lambda_{\theta o}\frac{h_c^{3}}{8}-r\lambda_{\theta i}\frac{h_c^{3}}{8}=0\\
&rQ^{c}_{sz,s}+Q^{c}_{\theta z,\theta}-R^{c}_{\theta}+N\left(w_c\right)+r\lambda_{zo}-r\lambda_{zi}=0\\
&rM^{c}_{Q1sz,s}+M^{c}_{Q1\theta z,\theta}-rR^{c}_{z}-M^{c}_{\theta1}-r\lambda_{zo}\frac{h_c}{2}-r\lambda_{zi}\frac{h_c}{2}=0\\
&rM^{c}_{Q2sz,s}+M^{c}_{Q2\theta z,\theta}-2rM^{c}_{z1}-M^{c}_{\theta2}+r\lambda_{zo}\frac{h_c^{2}}{4}-r\lambda_{zi}\frac{h_c^{2}}{4}=0\\
&rM^{c}_{Q3sz,s}+M^{c}_{Q3\theta z,\theta}-3rM^{c}_{z2}-M^{c}_{\theta3}-r\lambda_{zo}\frac{h_c^{3}}{8}-r\lambda_{zi}\frac{h_c^{3}}{8}=0
\end{aligned}
\tag{17}
$$

and six compatibility conditions corresponding to perfect bonding:

$$
\begin{aligned}
&u_{0o}+\frac{h_o}{2}\varphi^{o}_{s}-u_0+u_1\frac{h_c}{2}-u_2\frac{h_c^{2}}{4}+u_3\frac{h_c^{3}}{8}=0\\
&v_{0o}+\frac{h_o}{2}\varphi^{o}_{\theta}-v_0+v_1\frac{h_c}{2}-v_2\frac{h_c^{2}}{4}+v_3\frac{h_c^{3}}{8}=0\\
&w_o-w_0+w_1\frac{h_c}{2}-w_2\frac{h_c^{2}}{4}+w_3\frac{h_c^{3}}{8}=0\\
&u_0+u_1\frac{h_c}{2}+u_2\frac{h_c^{2}}{4}+u_3\frac{h_c^{3}}{8}-u_{0i}+\frac{h_i}{2}\varphi^{i}_{s}=0\\
&v_0+v_1\frac{h_c}{2}+v_2\frac{h_c^{2}}{4}+v_3\frac{h_c^{3}}{8}-v_{0i}+\frac{h_i}{2}\varphi^{i}_{\theta}=0\\
&w_0+w_1\frac{h_c}{2}+w_2\frac{h_c^{2}}{4}+w_3\frac{h_c^{3}}{8}-w_i=0
\end{aligned}
\tag{18}
$$

where $N\left(w_0\right), N\left(w_i\right)$ and $N\left(w_c\right)$ are defined in Appendix A.

5 SIMPLY-SUPPORTED BOUNDARY CONDITIONS

In this section, assumed the outer and the inner face sheets are simply-supported and the vertical displacements through the depth of the core at the edges of the sandwich cylinder are prevented, see Fig. 2. A Navier's solution method with twenty-eight trigonometric Fourier series, which satisfies the boundary conditions, is established. The Fourier series can be expressed as:

$$\begin{Bmatrix} u_{0j} \\ \varphi_s^j \\ u_K \\ \lambda_{sj} \end{Bmatrix} = \sum_{m=1}^{M}\sum_{n=1}^{N} \begin{Bmatrix} C_{uj} \\ C_{\varphi sj} \\ C_{uK} \\ C_{\lambda sj} \end{Bmatrix} \cos\left(\frac{m\pi}{L}s\right)\cos(n\theta) \qquad , \; j = o,i \quad , \; K = 0,1,2,3$$

$$\begin{Bmatrix} v_{0j} \\ \varphi_\theta^j \\ v_K \\ \lambda_{\theta j} \end{Bmatrix} = \sum_{m=1}^{M}\sum_{n=1}^{N} \begin{Bmatrix} C_{vj} \\ C_{\varphi\theta j} \\ C_{vK} \\ C_{\lambda\theta j} \end{Bmatrix} \sin\left(\frac{m\pi}{L}s\right)\sin(n\theta) \qquad , \; j = o,i \quad , \; K = 0,1,2,3 \tag{19}$$

$$\begin{Bmatrix} w_j \\ w_K \\ \lambda_{zj} \end{Bmatrix} = \sum_{m=1}^{M}\sum_{n=1}^{N} \begin{Bmatrix} C_{wj} \\ C_{wK} \\ C_{\lambda zj} \end{Bmatrix} \sin\left(\frac{m\pi}{L}s\right)\cos(n\theta) \qquad , \; j = o,i \quad , \; K = 0,1,2,3$$

where $C_{uj}, C_{vj}, C_{wj}, C_{\varphi sj}, C_{\varphi\theta j}, C_{uK}, C_{vK}, C_{wK}, C_{\lambda sj}, C_{\lambda\theta j}$ and $C_{\lambda zj}$ are the twenty-eight unknown constants of the Fourier series. In addition, *m* and *n* are the wave numbers and *M* and *N* are the number of terms in the Fourier series. After substitution of the Fourier series, Eqs. (19), into the equilibrium equations, Eqs. (15)– (18), along with the stress resultants of the functionally graded face sheets, and the high-order stress resultants of the core, the problem can be expressed in matrix form as:

$$[L]\{C\} = \{F\} \tag{20}$$

where $\{C\}$ vector contains twenty-eight unknown constants and components of $[L]$ matrix are not presented here for the sake of brevity, but nonzero components of $\{F\}$ vector are shown in Eq. (21). Eq. (27) is solved for $\{C\}$ by using MATLAB software, and the twenty-eight unknown constants are obtained.

$$\begin{aligned} &F(1) = -R.n_s^0 \;, F(3) = -N_{\theta\theta}^{T0} \;, F(4) = -R.n_s^i \;, F(6) = -N_{\theta\theta}^{Ti} \;, F(16) = -R_c^{cT} \;, \\ &F(17) = -R_c^{cT} - M_{c1}^{cT} \;, F(18) = -2RM_{c1}^{cT} - M_{c2}^{cT} \;, F(19) = -3RM_{c2}^{cT} - M_{c3}^{cT} \end{aligned} \tag{21}$$

where $R_c^{cT}, M_{c1}^{cT}, M_{c2}^{cT}, M_{c3}^{cT}$ are the thermal stresses resultants of the core and are defined as:

$$\begin{Bmatrix} R_c^{cT} \\ M_{c1}^{cT} \\ M_{c2}^{cT} \\ M_{c3}^{cT} \end{Bmatrix} = \int_{-h_c/2}^{h_c/2} \frac{E_c(T_c).\alpha_c(T_c).\Delta T_c}{1-\nu_c(T_c)} \begin{Bmatrix} 1 \\ z \\ z^2 \\ z^3 \end{Bmatrix} dz_c \tag{22}$$

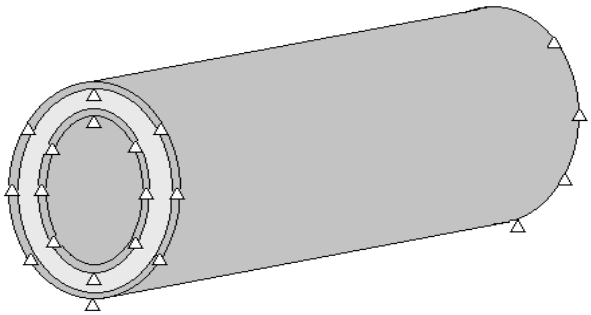

Fig.2
Three-dimensional view of sandwich cylinder with simply-supported boundary conditions.

6 NUMERICAL RESULTS AND VALIDATION

In this section, the numerical results of sandwich cylinders with FG face sheets are calculated for two types of ceramic and metal combinations as defined in Table 1. The material properties C in the FG face sheets can be expressed as a function of temperature as Eq. (2). Table 2, shows the temperature-dependent properties of constituent materials of Si3N4, Ni, ZrO2 and Ti–6Al–4V defined by five constants for third-order function of temperature that is introduced by Eq. (2), [41]. In two examples defined in Table 1, the outer surfaces of the FG face sheets are assumed to be ceramic rich (Si3N4 or ZrO2) and the FG face sheets in the face sheet-core interfaces are assumed to be pure metal (Ni or Ti–6Al–4V). In addition, numerical examples are simulated by ABAQUS software for validation of the present approach in special cases.

Table 1
Two examples of sandwich cylinder.

	FG face sheets	core
Type I	Silicon nitride/Nickel	Stainless steel
Type II	Zirconia/Titanium	Titanium

Table 2
Temperature-dependent properties of constituent materials of the FG face sheets [30].

	Si3N4			ZrO2		
	E	v	ρ	E	v	ρ
c_0	348.4323×10^{2}	0.24	2370	244.27×10^{2}	0.2882	3000
c_{-1}	0	0	0	0	0	0
c_1	-3.0697386×10^{-4}	0	0	-1.371×10^{-2}	1.133×10^{-4}	0
c_2	2.160186×10^{-7}	0	0	1.214×10^{-6}	0	0
c_3	-8.946165×10^{-11}	0	0	-3.681×10^{-9}	0	0
	Ni			Ti–6Al–4V		
c_0	223.95×10^{2}	0.31	8900	122.56×10^{5}	0.2884	4420
c_{-1}	0	0	0	0	0	0
c_1	-2.794×10^{-4}	0	0	-4.586×10^{-4}	1.122×10^{-4}	0
c_2	-3.998×10^{-9}	0	0	0	0	0
c_3	0	0	0	0	0	0

The critical dimensionless axial loads are shown in Table 3, for various temperatures. Table 3, shows this variation in a uniform temperature distribution for simply supported symmetric sandwich cylinders and for different power law indices, "N". The results are calculated by present formulations and also calculated by ABAQUS finite element code and then they are compared together. "H" is the total thickness of the sandwich cylinder, and the critical dimensionless axial load is defined as:

$$\bar{N}_{cr} = \frac{N_0}{E_{ce}.H} \tag{23}$$

where E_{ce} is Young's modulus of the homogeneous ceramic. As depicted in Table 3., while the temperature is increased, the critical dimensionless axial loads are decreased. Because, according to Eq. (2), increasing of the temperature, causes decreasing in the strength of the material. To clarify this phenomenon, the effect of temperature on the Young's modulus of ceramic and metal is indicated in Table 4. With increasing the temperature, elasticity modulus of metal and ceramic are decreased, but due to the microstructural reasons, decreasing the elasticity modulus of metal is more. Therefore, increasing the temperature reduces the mechanical properties, and it is one of the most important reasons in decreasing the critical dimensionless axial loads in high temperatures.

Table 3
Variation of critical dimensionless static axial load for type I and type II sandwich cylinders with different T and N ($\frac{R}{H}=300, h_c/h_0=10, \frac{L}{R}=2$).

$T(K)$	$\bar{N}_{cr}\times10^3$							
	Type I				Type II			
	N=0	*N*=1	*N*=2	*N*=3	N=0	*N*=1	*N*=2	*N*=3
300	2.143	1.991	1.897	1.983	1.692	1.563	1.495	1.547
ABAQUS	2.098	1.861	1.803	2.052	1.675	1.552	1.368	1.419
Discrepancy (%)	2.14	6.98	5.21	3.36	1.01	0.708	9.283	9.02
400	2.012	1.890	1.798	1.860	1.547	1.465	1.423	1.460
ABAQUS	1.896	1.711	1.624	1.692	1.479	1.321	1.278	1.326
Discrepancy (%)	6.11	10.46	10.71	9.92	4.59	10.9	11.34	10.10
500	1.887	1.784	1.703	1.771	1.465	1.390	1.323	1.381
ABAQUS	1.802	1.705	1.616	1.677	1.413	1.310	1.198	1.302
Discrepancy (%)	4.71	4.63	5.38	5.60	3.68	6.10	10.43	6.06

Table 4
Effect of temperature variation on the Young modulus in metal and ceramics.

T	Silicon Nitride	Zirconium dioxide
300 *K*	322.27 (*GPa*)	168.06 (*GPa*)
1500 *K*	252.14 (*Gpa*)	105.68 (*GPa*)
Change	21.76%	37.11%

Critical dimensionless axial loads in Table 5, are calculated in different core thickness-to-face sheet thickness ratio h_c/h_0 for different property distributions of the FG face sheets and also for two types of sandwich cylinders, type I and type II. In various indices, "*N*", raising the core thickness-to-face sheet thickness ratio causes the critical dimensionless axial loads decrease. Because, with increasing h_c/h_0 ratio, the thickness of the core will be bigger and so the structure will be weaker.

Table 5
Variation of critical dimensionless static axial load for type I and type II sandwich cylinders with different h_c/h_0 and N ($\frac{R}{H}=300, \frac{L}{R}=2$).

h_c/h_0	$\bar{N}_{cr}\times10^3$							
	Type I				Type II			
	N=0	*N*=1	*N*=2	*N*=3	*N*=0	*N*=1	*N*=2	*N*=3
5	2.579	2.245	2.037	2.153	1.796	1.610	1.513	1.593
ABAQUS	2.412	2.073	1.814	2.017	1.726	1.565	1.486	1.552
10	2.317	2.055	2.001	2.069	1.735	1.551	1.507	1.548
ABAQUS	2.226	1.955	1.758	1.901	1.675	1.492	1.478	1.522
15	2.125	1.957	1.935	1.980	1.689	1.505	1.491	1.504
ABAQUS	1.984	1.860	1.749	1.841	1.633	1.468	1.456	1.486

Tables 3 and 5 indicate with changing the property distribution of the FG face sheets from linear to quadratic; the critical dimensionless axial load $\bar{N}_{cr}$ is decreased, because, more percent of the face sheets materials changes to metal and stiffness structure is lower and so the critical dimensionless axial load is decreased. But, $\bar{N}_{cr}$ is increased with changing the property distribution of the FG face sheets from quadratic to cubic distribution. Because, more percent of the face sheet materials changes to ceramic and stiffness structure is higher and so the critical dimensionless axial load is increased.

Also, the constituents of type I is stronger than type II and their young modulus are bigger than type II so the critical dimensionless axial loads of type I sandwich cylinder are generally bigger than the critical dimensionless axial loads of type II.

In Table 6., variation of critical dimensionless static axial load for type I and type II sandwich cylinders with different compositional profiles N and different ratio R/H are presented. They are calculated numerically (by

ABAQUS) and analytically (by present formulation). When the ratio R/H is increased, the value of the critical dimensionless static axial load is decreased. Furthermore, Tables 3, 4 and 6 indicate that the numerical results and the analytical results are in a good agreement.

In order to simulating the structure in Abaqus software, the thickness of the FG face sheets is divided into 20 layers. Then, isotropic mechanical properties are assumed for each layer which is gradually change from pure metal on one surface to the pure ceramic on the other surface according to the FG power law distribution.

Table 6

Variation of critical dimensionless static axial load for type I and type II sandwich cylinders with different $\frac{R}{H}$ and N ($h_c/h_0=10, \frac{L}{R}=2$).

	$\bar{N}_{cr}\times10^3$							
$\frac{R}{H}$	Type I				Type II			
	N=0	*N*=1	*N*=2	*N*=3	*N*=0	*N*=1	*N*=2	*N*=3
200	2.721	2.553	2.467	2.596	2.423	1.914	1.337	1.910
ABAQUS	2.486	2.219	2.100	2.189	2.202	1.663	1.164	1.658
400	1.425	1.273	1.231	1.270	1.321	0.962	0.928	0.957
ABAQUS	1.254	1.146	1.002	1.078	1.032	0.899	0.805	0.825
600	0.935	0.850	0.819	0.844	7.312	0.639	0.618	0.641
ABAQUS	0.895	0.781	0.753	0.756	6.985	0.556	0.551	0.531

In Figs. 3(a) and 4(a), the variations of the critical dimensionless axial loads are depicted with length to radius ratios for type I and type II, respectively. Furthermore, in Figs.3 (b) and 4(b), the variations of the critical dimensionless axial loads are depicted with wave number changing for type I and type II, respectively. All these figures are plotted for four values of power law indices, *N*=0, 0.2, 1, 2. In Figs. 3 and 4, with increasing the length to radius ratios and with increasing the wave number, the critical dimensionless axial loads are decreased. In addition, Figs. 3 and 4 depict that in a constant temperature, the critical dimensionless axial loads are decreased with increasing the power law index from *N*=0 to *N*=2. Because, with increasing the power-law index from *N*=0 to *N*=2, the properties of the FG face sheets are near to metal properties and the strength of the structure is decreased.

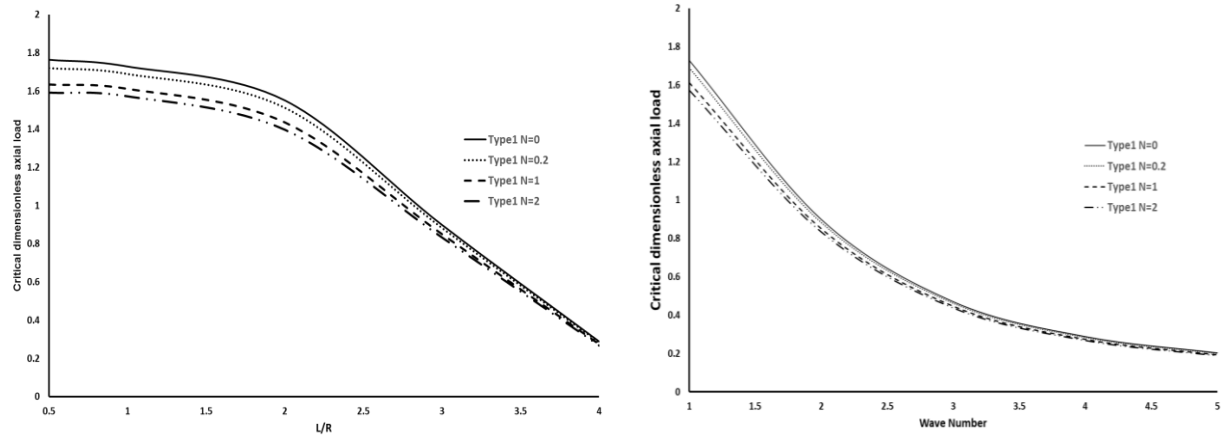

(a) (b)

Fig.3
a) Variation of critical dimensionless axial load via *L/R* for various power law indices (Type I). b) Variation of critical dimensionless axial load via wave numbers for various power law indices (Type I).

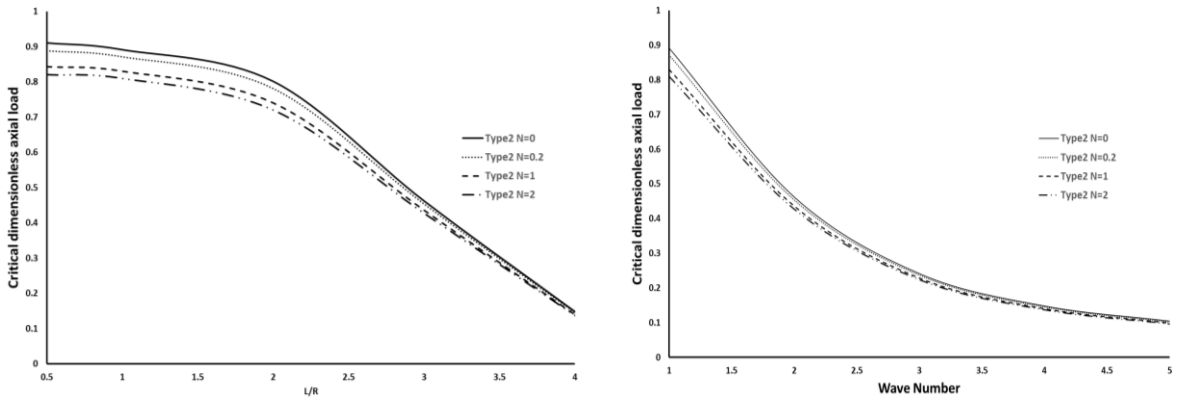

(a) (b)

Fig.4
a) Variation of critical dimensionless axial load via *L/R* for various power law indices (Type II). b) Variation of critical dimensionless axial load via wave numbers for various power law indices (Type II).

7 CONCLUSION

The buckling of sandwich cylinders with functionally graded face sheets subjected to axial compressive load is studied. The temperature dependent material properties of FG face sheets are varied by power-law distribution along the thickness. The results show the critical dimensionless static axial loads are affected by the configurations of the constituent materials, compositional profile variations, temperature and the variation of the sandwich geometry. Based on the results obtained, the important results are as follows. When the ratio R/H is increased, the critical dimensionless static axial loads are decreased. In addition, for all cases, when the property distribution changes linearly and cubic, the values of critical dimensionless static axial load are nearly the same. When temperature *T* and core thickness-to-face sheet thickness ratio h_c/h_0 are increased, the value of critical dimensionless axial load is decreased. With increasing the *L/R* ratio, value of critical dimensionless axial load is decreased. And finally, by increasing the wave number, the critical dimensionless axial loads are decreased.

APPENDIX A

$N\left(w_0\right), N\left(w_i\right)$ and $N\left(w_c\right)$ are defined as follows:

$$N\left(w_j\right)=\hat{N}_{ss}^{j}.rw_{j,ss} \quad , \; j=(o,i,c) \tag{A.1}$$

And $\hat{N}_{ss}^{0}, \hat{N}_{ss}^{i}$ and $\hat{R}_s^c$ are the parts of total external load, $\hat{N}_0$ which are exerted to the outer face sheet, inner face sheet and the core along s direction, respectively.

$$\hat{N}_{ss}^{o}+\hat{N}_{ss}^{i}+\hat{R}_s^c=-\hat{N}_0 \tag{A.2}$$

In this analysis, uniform state of strain for the face sheets and the core is assumed. With this assumption and a little simplification, we can write:

$$\frac{\hat{N}_{ss}^{o}}{h_o\bar{E}_o}=\frac{\hat{N}_{ss}^{i}}{h_i\bar{E}_i}=\frac{\hat{R}_s^c}{h_cE_c} \tag{A.3}$$

where E_c is the elasticity modulus of the core; and $\bar{E}_o$ and $\bar{E}_i$ are the equilibrium elasticity modulus in the outer and inner face sheet, respectively, that are defined as:

$$\bar{E}_o = \frac{\int_{-h_o/2}^{h_o/2} E_o(z_o)dz_o}{h_o} \quad , \quad \bar{E}_i = \frac{\int_{-h_i/2}^{h_i/2} E_i(z_i)dz_i}{h_i} \tag{A.4}$$

Hence, with use of Eqs. (A.2) and (A.3), the external in-plane loads exerted to the face sheets and the core along *s* direction can be calculated as:

$$\begin{Bmatrix} \hat{N}_{ss}^{o} \\ \hat{N}_{ss}^{i} \\ \hat{R}_{s}^{c} \end{Bmatrix} = \frac{-\hat{N}_0}{h_o\bar{E}_o + h_i\bar{E}_i + h_cE_c} \begin{Bmatrix} h_o\bar{E}_o \\ h_i\bar{E}_i \\ h_cE_c \end{Bmatrix} \tag{A.5}$$

REFERENCES

[1] Suresh S., Mortensen A., 1998, *Fundamentals of Functionally Graded Materials*, Barnes and Noble Publisher, London.

[2] Plantema F.G., 1966, *Sandwich Construction*, John Wiley & Sons Inc., New York.

[3] Allen H.G., 1969, *Analysis and Design of Structural Sandwich Panels*, Pergamon Press Inc., New York.

[4] Zenkert D., 1995, *An Introduction to Sandwich Construction*, Chameleon Press, London.

[5] Javaheri R., Eslami M. R., 2002, Thermal buckling of functionally graded plates, *AIAA Journal* **40**(1): 162-169.

[6] Zhao X., Lee Y. Y., Liew K. M., 2009, Mechanical and thermal buckling analysis of functionally graded plates, *Composite Structures* **90**(2): 161-171.

[7] Amir S., Khorasani M., BabaAkbar-Zarei H., 2018, Buckling analysis of nano composite sandwich plates with piezoelectric face sheets based on flexoelectricity and first-order shear deformation theory, *Journal of Sandwich Structures & Materials* **2018**: 109963621879538.

[8] Bouderba B., Houari M.S.A., Tounsi A., Mahmoud S.R., 2016, Thermal stability of functionally graded sandwich plates using a simple shear deformation theory, *Structural Engineering and Mechanics* **58**(3): 397-422.

[9] Amir S., 2016, Orthotropic patterns of visco-Pasternak foundation in nonlocal vibration of orthotropic graphene sheet under thermo-magnetic fields based on new first-order shear deformation theory, *Proceedings of the Institution of Mechanical Engineers, Part L: Journal of Materials: Design and Applications.*

[10] Sepiani H.A., Rastgoo A., Ebrahimi F., Arani A.G., 2010, Vibration and buckling analysis of two-layered functionally graded cylindrical shell, considering the effects of transverse shear and rotary inertia, *Materials & Design* **31**(3): 1063-1069.

[11] Amir S., Bidgoli E.M.R., Arshid E., 2018, Size-dependent vibration analysis of a three-layered porous rectangular nano plate with piezo-electromagnetic face sheets subjected to pre loads based on SSDT, *Mechanics of Advanced Materials and Structures* **2018**: 1-15.

[12] Frostig Y., Baruch M., Wilnay O., Shienman I., 1992, High-order theory for sandwich-beam behavior with transversely flexible core, *Journal of Engineering Mechanics* **118**(5): 1026-1043.

[13] Frostig Y., Baruch M., 1994, Vibration of sandwich beams-a high-order theory approach, *Journal of Sound and Vibration* **176**(2): 195-208.

[14] Bozhevolnaya E., Frostig Y., 2001, Free vibration of curved sandwich beams with a transversely flexible core, *Journal of Sandwich Structures and Materials* **3**: 311-342.

[15] Bozhevolnaya E., Sun J.Q., 2004, Free vibration analysis of curved sandwich beams, *Journal of Sandwich Structures and Materials* **6**: 47-76.

[16] Frostig Y., Thomsen O.T., 2004, High-order free vibration of sandwich panels with a flexible core, *International Journal of Solids and Structures* **41**: 1697-1724.

[17] SchwartsGivli H., Rabinovitch O., Frostig Y., 2008, Free vibration of delaminated unidirectional sandwich panels with a transversely flexible core and general boundary conditions-a high-order approach, *Journal of Sandwich Structures and Materials* **10**: 99-131.

[18] Mohammadi Y., Khalili S.M.R., 2011, Effect of geometrical and mechanical properties on behavior of sandwich beams with functionally graded face sheets under indentation loading, *Journal of Materials: Design and Applications* **225**: 231-244.

[19] Seidi J., Khalili S.M.R., Malekzadeh K., 2015, Temperature-dependent buckling analysis of sandwich truncated conical shells with FG face sheets, *Composite Structures* **131**: 682-691.

[20] Flu W., 1973, *Stresses in Shells*, Springer-Verlag, New York.

[21] Bush B.O., Almroth B.O., 1975, *Buckling of Bars, Plates and Shells*, McGraw-Hill, New York.

[22] Theodore von K., Hsue-Shen T., 1941, The buckling of thin cylindrical shells under axial compression, *Journal of the Aeronautical Sciences* **8**(8): 303-312.
[23] Winterstetter T.A., Schmidt H., 2002, Stability of circular cylindrical shells under combined loading, *Journal of Thin-Walled Structures* **40**: 893-909.
[24] Kim S.E., Kim C.S., 2002, Buckling strength of cylindrical shell and tank subjected to axially compressive loads, *Journal of Thin-Walled Structures* **40**: 329-353.
[25] Pinna R., Ronalds B.F., 2002, Buckling and post-buckling of shells with one end pinned and the other end free, *Journal of Thin-Walled Structures* **40**: 507-525.
[26] Ru C.Q., 2000, Effect of van der Waals force on axial buckling of a double walled carbon nanotube, *Journal of Applied Physics* **87**: 7227-7231.
[27] Eslami M.R., Javaheri R.,1999, Buckling of composite cylindrical shells under mechanical and thermal loads, *Journal of Thermal Stresses* **22**: 527-545.
[28] Eslami M.R., Shahsiah R.,2001, Thermal buckling of imperfect cylindrical shells, *Journal of Thermal Stresses* **24**: 71-89.
[29] Mushtari K.M., Sachenkov A.V., 1958, Stability of cylindrical and conical shells of circular cross section with simultaneous actin of axial compression and external normal pressure, *NACA TM* **1433**: 667-674.
[30] Lopatin A.V., Morozov E.V., 2015, Buckling of the composite sandwich cylindrical shell with clamped ends under uniform external pressure, *Journal of Composite Structures***122**: 209-216.
[31] Malinowski M., Belica T., Magnucki K., 2015, Bucklingandpost-buckling behavior of elastic seven-layered cylindrical shells – FEM study, *Journal of Thin-Walled Structures* **94**: 478-484.
[32] Hui-Shen S., 2002, Postbuckling analysis of axially-loaded functionally graded cylindrical shells in thermal environments, *Journal of Composites Science and Technology* **62**: 977-987.
[33] Hui-Shen S., 2003, Postbuckling analysis of pressure-loaded functionally graded cylindrical shells in thermal environments, *Journal of Engineering Structures* **22**: 977-987.
[34] Lis R., Batra R.C., 2006, Buckling of axially compressed thin cylindrical shells with functionally graded middle layer, *Journal of Thin-Walled Structures* **44**: 1039-1047.
[35] Sofiyev A.H., 2014, The vibration and buckling of sandwich cylindrical shells covered by different coatings subjected to the hydrostatic pressure, *Journal of Composite Structures* **117**: 124-134.
[36] Shahsiah R., Eslami M.R., 2003, Functionally graded cylindrical shell thermal instability based on improved donnell equations, *AIAA Journal* **41**: 19-26.
[37] Woo J., Meguid S.A., Stranart J.C., Liew K.M., 2005,Thermo mechanical post buckling analysis of moderately thick functionally graded plates and shallow shells, *International Journal of Mechanical Sciences* **47**: 1147-1171.
[38] Ravikiran K., Ganesan N., 2006, Buckling and free vibration analysis of functionally graded cylindrical shells subjected to a temperature-specified boundary condition, *Journal of Sound and Vibration* **289**: 450-480.
[39] Khalili S.M.R., Mohammadi Y., 2012, Free vibration analysis of sandwich plates with functionally graded face sheets and temperature-dependent material properties: A new approach, *European Journal of Mechanics A/Solids* **35**: 61-74.
[40] Reddy J.N., 2012, *Thermal Mechanical Behavior of Functionally Graded Materials*, Texas.
[41] Mohammadi Y., Khalili S.M.R., Malekzadeh Fard K., 2016, Low velocity impact analysis of sandwich plates with functionally graded face sheets, *Mechanics of Advanced Materials and Structures* **23**(4): 363-374.